Journal of Food Engineering 410 (2026) 112916

Contents lists available at ScienceDirect

Journal of Food Engineering

journal homepage: www.elsevier.com/locate/jfoodeng

3D structure of protein networks and lipid globules in heat-treated egg yolk revealed by X-ray holo-tomography

Felix Wittwer [a,b,*], Nimmi Das Anthuparambil [b], Frederik Unger [b], Randeer Pratap Gautam [b], Silja Flenner [c], Imke Greving [c], Christian Gutt [b], Peter Modregger [a,b]

[a] Deutsches Elektronen-Synchrotron DESY, Notkestraße 85, 22607 Hamburg, Germany
[b] Department Physik, Universität Siegen, Walter-Flex-Straße 3, 57072 Siegen, Germany
[c] Helmholtz-Zentrum Hereon, Max–Planck-Straße 1, 21502 Geesthacht, Germany

ARTICLE INFO

Keywords:
Liquid–liquid phase separation
X-ray holography
Tomography
Egg yolk
Food science

ABSTRACT

Upon heating, egg yolk transforms from a liquid to a grainy gel due to a combination of lipid aggregation, protein denaturation–aggregation–gelation and other processes. This heat-induced solidification of egg yolk can serve as a useful model system for the investigation of protein denaturation and gelation in biological systems in general. Using X-ray holographic tomography, we studied the heat-induced changes in egg yolk on the micron to sub-micron length scale. In contrast to electron microscopy, X-ray holography does not require sample staining, fixation, or drying, which potentially alter the sample and harm sample fidelity. Our results reveal a developing separation between proteins and lipids with fatty components rapidly aggregating into large globules around 40 μm in diameter.

1. Introduction

Egg yolk is widely used as a versatile ingredient in cooking and food processing. It serves as a natural emulsifier, binding fats and water to create smooth textures in sauces, dressings, and baked goods. Beyond its culinary appeal, egg yolk is packed with essential nutrients, including proteins, lipids, vitamins, and minerals (Huopalahti et al., 2007). Cooking egg yolk involves a fascinating transformation of its proteins and lipids (Anthuparambil et al., 2023). When heated, egg yolk undergoes denaturation, aggregation, coagulation and gelation, leading to changes in texture and consistency (Anthuparambil et al., 2023; Anton, 2013). The final texture depends sensitively on factors such as temperature and heating rate. In general, the microstructure of a protein gel defines its viscoelasticity, with the resulting mechanical, interfacial, and transport properties being crucial for various applications in bio-nanotechnology and food industry (Mine, 2008).

Although the liquid-to-gel transformation of egg yolk is a well-known phenomenon, the evolution of its microstructure during denaturation-aggregation-gelation processes is not yet fully understood. In the past, electron microscopy (EM) has been used to study the microstructure of gelatinous egg yolk (Cordobés et al., 2004; Aguilar et al., 2019) and the aggregation of lipids (Bellairs, 1961; Hsu et al., 2009). However, EM studies require chemical fixation of the sample, which can lead to sample degradation and distorted results (Běhalová et al., 2020; Nikara et al., 2020). Additionally, transmission EM requires ultra-thin sectioning of samples due to the limited penetration depth of electrons. In contrast, x-rays can penetrate deep into biological tissues and materials, providing a more comprehensive structural analysis while preserving the sample's integrity.

In previous works (Anthuparambil et al., 2023, 2024), we used low-dose x-ray photon correlation spectroscopy (XPCS) to investigate the functional contribution of yolk components, mainly plasma proteins, low-density lipoproteins (LDL), and egg yolk granules, to the formation of the grainy-gel microstructure under heat induction. We found that at temperatures above 75 °C, two kinds of structure formation occur in egg yolk. Egg yolk plasma proteins form a gel network and LDLs form aggregates, which are embedded in the protein gel network. However, using small-angle and ultra-small-angle scattering, these studies could only provide insight into structure sizes smaller than 600 nm, which is not large enough to resolve the $\gtrsim 1\,\mu m$ features of the protein-LDL aggregate microstructure that form at higher temperatures or longer heating times.

X-ray tomography allows to study the internal structure of samples without requiring destructive or harmful sample preparation (Withers et al., 2021). Conventional x-ray tomography measures the absorption contrast of the sample, which is negligible for soft, biological materials such as cooked egg yolk. For these samples, x-ray phase contrast

* Corresponding author at: Deutsches Elektronen-Synchrotron DESY, Notkestraße 85, 22607 Hamburg, Germany.
E-mail address: felix.wittwer@desy.de (F. Wittwer).

https://doi.org/10.1016/j.jfoodeng.2025.112916
Received 6 August 2025; Received in revised form 12 November 2025; Accepted 9 December 2025
Available online 12 December 2025

imaging has become the state of the art as the phase contrast can be hundreds of times larger than the absorption contrast (Paganin and Pelliccia, 2021). This allows phase contrast methods such as x-ray holography to measure small contrast differences with a minimal radiation dose to the sample (Flenner et al., 2020). Using x-ray holography, we achieved a resolution of 200 nm, which is complementary to our previous XPCS results and allows to relate the microtopology with the collective dynamics. By measuring egg yolk samples heated for different time durations, we were able to image the evolution of protein networks and lipid aggregation.

This article is organized as follows: In Section 2, we describe the experimental details, grouped into sample preparation, measurement and data reconstruction; In Section 3, we describe the observed evolution of the protein networks during heating; In Section 4, we report the formation of lipid globules, their transformation and provide a hypothesis for their evolution; In Section 5 we summarize and discuss the results.

2. Experimental details

2.1. Sample preparation

The egg yolk used in this study was extracted from a hen egg purchased from a local supermarket. The egg yolk was separated from the egg white using a steel strainer and washed with Milli-Q water to remove any residual albumen. The cleaned yolk was placed on filter paper to absorb excess water and albumen. To ensure the complete removal of the albumen, the yolk was gently rolled on the filter paper several times. Then, the vitelline membrane was punctured using a plastic pipette tip, and the yolk was extracted and stored in a 15 mL Falcon tube at 5 °C.

For the tomography experiments, the yolk was filled into Kapton capillaries of three diameters, coined *small*, *intermediate*, and *medium*. The capillaries have a wall thickness of 0.025 mm and inner diameters of 0.12 mm, 0.25 mm, and 0.5 mm, respectively. After filling the capillaries, both ends were closed using epoxy glue.

The sealed sample capillaries were dipped in boiling water at 100 °C for heating times of up to 22 min. After heating for a specific time, the samples were immediately quenched to low temperatures to stop further changes by dipping in cooled water at ≈ 5 °C. Afterwards, the sample capillaries were glued onto a vertical pin which was then mounted onto the sample holder for tomographic studies. The samples remained sealed in the capillaries with no further sample fixation necessary. The sample preparation was usually much quicker than the measurement process because most samples were prepared in batches. This led to varying waiting times between sample preparation and measurement, sometimes more than an hour.

2.2. Measurements

We performed the measurements at the P05 beamline operated by the Helmholtz-Zentrum Hereon at PETRA III, using the holo-tomography setup pictured in Fig. 1 (Flenner et al., 2022). The setup used a Si-111 channel-cut monochromator to select an x-ray energy of 11 keV. To resolve features smaller than one micrometer, the setup used a cone beam geometry to project an enlarged image of the sample onto the detector. The cone beam was formed using a Fresnel zone plate (FZP) with a diameter of 300 µm and an outermost zone width of 50 nm, a beamstop, and an order-sorting aperture (OSA). The sample was installed on a rotation stage 145.4 mm downstream of the focal plane. After irradiating the sample, the x-rays propagated through an evacuated pipe to the detector camera installed 19.6 m downstream of the focal plane. This resulted in a geometric magnification

$$M = \frac{19.6\,\mathrm{m}}{145.4\,\mathrm{mm}} = 135. \tag{1}$$

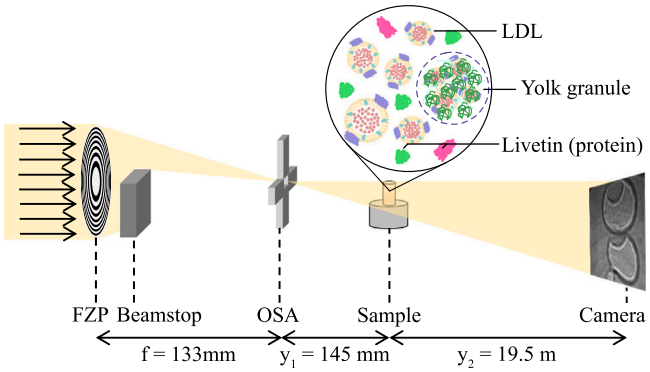

Fig. 1. The holo-tomography setup at the P05 beamline at PETRA III, DESY. The main components are a Fresnel zone plate (FZP) to focus the x-rays, a beamstop to block parts of the incident x-rays and an order-sorting aperture (OSA) to remove unwanted diffraction orders of the FZP. The sample is placed out of focus to project a magnified image on the camera. The zoom-in sketch shows the main components of raw egg yolk: low-density lipoproteins (LDL), yolk granules and livetin proteins (Huopalahti et al., 2007). LDLs are spherical particles with diameters of around 30 nm. They have a lipid core of triglycerides and cholesterol esters that is surrounded by a shell of phospholipids and apolipoproteins. Yolk granules are circular complexes with diameters ranging from 0.3 µm to 2 µm that contain LDLs, high-density lipoproteins and the protein phosvitin (Anton, 2013).

The holograms were recorded using a 10 µm-thick Gadox scintillator that was directly coupled to a Hamamatsu C12849-101U sCMOS camera. The camera had 2048 × 2048 pixels with a pixel size of 6.5 µm. For data processing, the pixels were binned 2 × 2, resulting in a pixel size of 13 µm and an image size of 1024 × 1024 pixels. Using the magnification of the cone beam, the setup achieved an effective pixel size $p = 13\,\mu\mathrm{m}/M = 96\,\mathrm{nm}$ in the sample plane with an effective field of view (FOV) of 98 µm. Because this FOV was too small to image the 170 µm-wide sample capillary, we used local tomography to record only a 98 µm-diameter cylinder of the capillary center. For each tomogram scan, the sample was rotated over 180° at a constant speed of 0.125° per second. While the sample was rotated, the camera recorded holograms with an exposure time of 0.8 s to ensure that no blurring occurred in the images. With a small overhead between each exposure, we could measure 1776 holograms for each tomogram. Based on the studies of Howells et al. (2009), we estimate that the required dose to resolve 100 nm details in a protein sample is around 100 kGy while the maximum tolerable dose is in the range of gigagray. For our measurements, one tomogram exposed the sample to 170 kGy, close to the minimum and far below the tolerable dose.

2.3. Data reconstruction

Each hologram was automatically reconstructed on the Maxwell computing cluster using the Holowizard package to obtain phase projections of the sample (Dora et al., 2024b, 2025, 2024a). From the phase projections we reconstructed the 3D phase shift of the sample using the P05 reconstruction pipeline based on TomoPy (Gürsoy et al., 2014). The pipeline used a gridrec algorithm with a Shepp–Logan filter and Fourier-wavelet ring removal. Following Diaz et al. (2012), the phase shift ϕ in each volume element (voxel) of the reconstructed volumes is related to the local electron density n_e by the classical electron radius r_0, the wavelength λ and the pixel size p:

$$n_e = -\frac{\phi}{r_0 \lambda p}. \tag{2}$$

Because the data was measured with local tomography, there is no absolute reference to calibrate the phase offset. Without knowing the

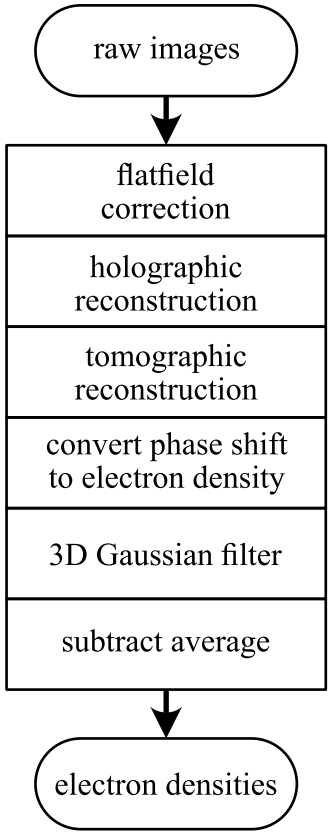

Fig. 2. Workflow diagram of the reconstruction pipeline.

absolute phase offset, we normalized the data by subtracting the average phase of each measurement. This normalization is based on the assumption that the average phase shift is the same for every sample. To suppress noise, we applied a 3D Gaussian filter with a standard deviation of $2p$ to the reconstructed volumes. A diagram of the workflow is shown in Fig. 2.

3. Evolution of protein networks

3.1. Network evolution

Liquid, raw egg yolk is difficult to measure with tomography because different parts of the liquid follow the rotation differently. In our measurements, only egg yolk that was heated for at least two minutes was stiff enough to successfully record a tomogram. Fig. 3 shows $25\,\mu m \times 25\,\mu m$ sections from the tomographic reconstructions of six egg yolk samples. The images show the deviation of the local electron density from the average electron density in each sample.

As the proteins aggregate during heating, they form compact, protein-rich domains that expel fat. Given that proteins contain a higher proportion of atoms with greater atomic numbers (e.g., nitrogen and oxygen) relative to lipids, these regions exhibit an elevated local electron density. The fat-rich domains on the other hand, primarily composed of lower-molecular weight hydrocarbon chains, exhibit a reduced local electron density. Accordingly, light structures indicate higher protein concentrations while dark regions indicate higher fat concentrations. For longer heating times, the size of the protein- and fat-rich regions grows, indicating a more pronounced separation as the protein network grows.

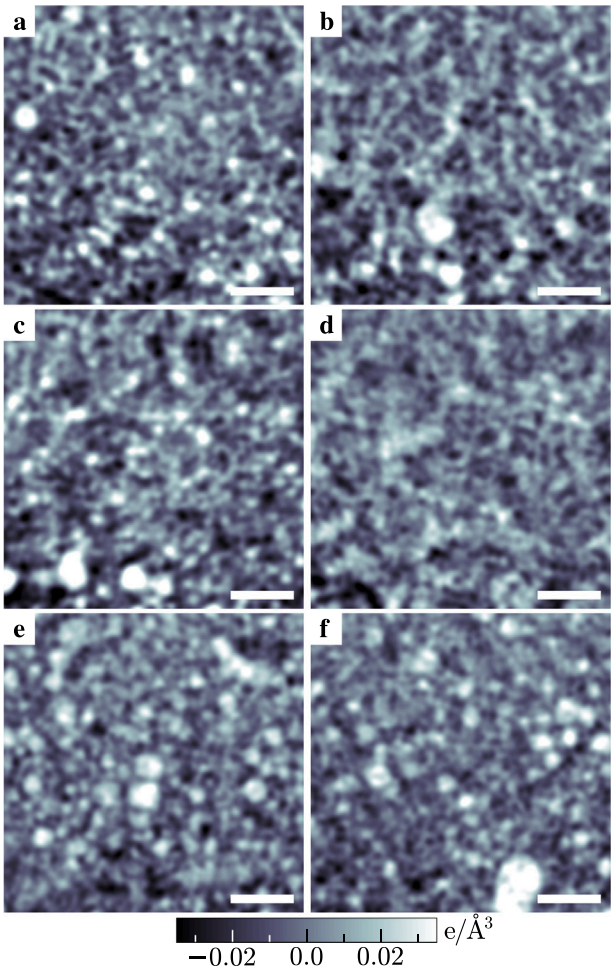

Fig. 3. Reconstructed slices of egg yolk samples in small capillaries. Shown is the local electron density minus the average density of each sample to highlight deviations. Light regions correspond to regions of high density, darker regions to low-density regions. For egg yolk, protein has the highest density and fat has the lowest density. The samples were heated for (a) 2 min, (b) 3 min, (c) 4 min, (d) 5 min, (e) 6 min, (f) 7 min. Because the average value has been subtracted, all slices share the same color scale. To reduce pixel-to-pixel noise, the slices have been denoised with a 2-pixel 3D Gaussian filter. The scale bars indicate 5 µm.

3.2. Structure analysis

To analyze the morphology of the protein networks, we extracted the network structure from the reconstructed volumes. To avoid potential edge artifacts from local tomography, we extracted from each reconstruction a $356 \times 356 \times 356$ voxel volume, which corresponds to a $34.2\,\mu m \times 34.2\,\mu m \times 34.2\,\mu m$ cube. We subtracted an estimated background from each volume to improve the correct classification of the network. Because the feature size of the network was not larger than a few micrometer, we estimated the background by filtering the data with a $10p$ 3D Gaussian filter. With the background removed, we converted the data to a binary mask by setting all positive voxels to one and the rest to zero, see Fig. 4(b). From the binary mask, we extracted the structure of the network using the skeletonize function from scikit-image (van der Walt et al., 2014), shown in Fig. 4(c). Finally, to extract the structure size, we segmented the space in the network using the watershed function from scikit-image, see Fig. 4(d). A diagram of the segmentation workflow is shown in Fig. S1 in the supplementary material.

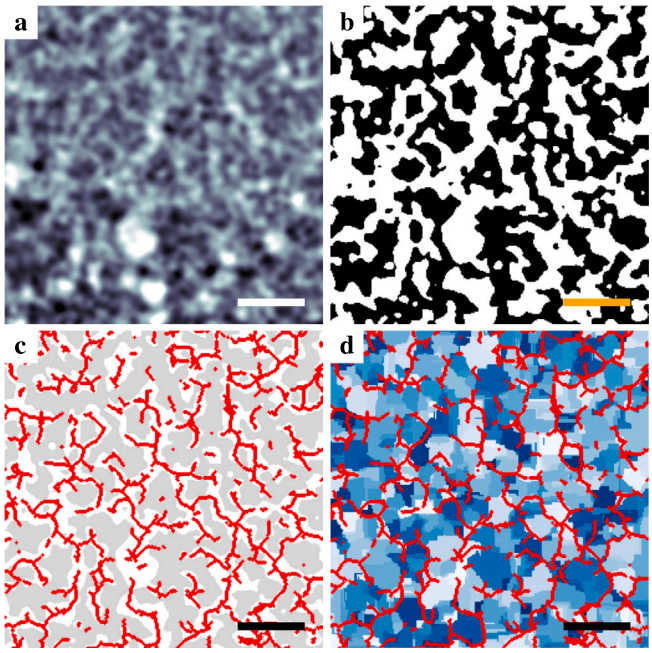

Fig. 4. (a) Reconstructed slice from the 3 min-heated egg yolk sample shown in Fig. 3b. (b) Threshold applied to the slice shown in (a), white areas are greater than the average, black areas are smaller than the average. (c) Extracted network shown in red with the thresholded slice in the background. The shown network combines ten neighboring slices to improve visibility. (d) Segmented space between the network, each segment shows a different blue color. The network is overlaid in red. All scale bars indicate 5 µm.

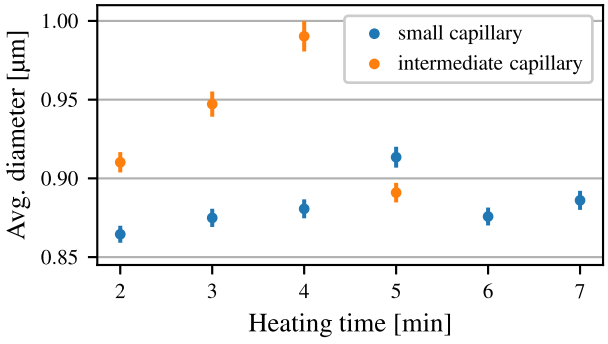

Fig. 5. Structure size in different heat-treated egg yolk samples. The data points show the average diameter of the space segments in each network, the error bars indicate the standard error of the average. To reduce edge effects, we calculated the average over the central $256 \times 256 \times 256$ voxels of each volume, which corresponds to a $24.6\,\mu m \times 24.6\,\mu m \times 24.6\,\mu m$ cube.

To compare different samples, we choose to calculate the average diameter of the segments in each network. The results for two sample batches are shown in Fig. 5. The first batch used small capillaries and contains time steps from two to seven minutes. The second batch used intermediate-sized capillaries and time steps from two to five minutes. Example sections from the first batch are shown in Fig. 3, sections from the second batch are included in the supplementary material.

While Fig. 5 hints at the general temporal evolution of the network structure, we also observe considerable variation across different measurements. These discrepancies in the apparent growth and size of the network may reflect underlying factors such as differences in sample preparation, local inhomogeneities, or subtle variations in the thermal or mechanical treatment protocols. Rather than indicating a single, well-defined pathway of network formation, our data suggest a complex and possibly sensitive assembly process, where the observed structural features can be strongly influenced by experimental conditions.

4. Evolution of lipid globules

4.1. Globule formation

After heating, some egg yolk samples showed small lipid aggregations. Because the sample preparation was much quicker than the time it took to collect one tomogram, many samples had to be stored after preparation until they could be measured. The samples were stored at room temperature, sometimes for more than an hour. In some of the samples, the small aggregations developed into large lipid globules while stored.

Fig. 6 shows four exemplary scans, arranged according to our estimated evolution of the lipid globules. In the first three columns, the egg yolk was inside small capillaries and heated for 6 min, 1.5 min, and 4 min, respectively. The sample shown in Fig. 6d was in a medium capillary and heated for 22 min.

Heating egg yolk not only denaturates the proteins but also affects the LDLs. At higher temperatures, the phospholipid shell of the LDLs becomes more permeable and can release the lipids inside. According to our estimated timeline, the LDLs agglomerate and form large globules. Remarkably, many of these globules have exactly one intrusion, see Fig. 6(a). As the intrusions grow, the globules become hollow and fill with the gel, see Fig. 6(b). It is notable that the intrusions are highly spherical, independent of the size and outer shape of the globule. This trend continues until the gel intrusions fill out most of the globule, see Fig. 6(c). Remarkably, the intrusions are still spherical at this stage, although the outer shape has become prolate. The circular shape of the intrusion points to a strong surface tension at the interface. At the end of the globule evolution, the lipid shell becomes thin and bubble-like, see Fig. 6(d). These thin structures appear only weakly in the projection, Fig. 6(d1), but are readily apparent in the tomographic slice, Fig. 6(d2). As the globules grow, they probably come into contact with neighboring globules but do not seem to merge together. Instead, they remain separated by a wall that is straight or has only a low curvature. When three walls meet, the angles between the walls are near 120°, exemplary indicated by the marker in Fig. 6(d2). These angles are congruent with Plateau's laws for bubble surfaces at equilibrium (Ball, 2011) and also indicative of a strong surface tension. Fig. 6(a3) and (b3) show enlarged sections of lipid globules and highlight that the protein network permeates through some of the lipid globules.

4.2. Hypothesis of globule evolution

The lipoproteins in raw egg yolk are about 30 nm in diameter (Evans et al., 1974) with a surface-to-volume ratio (SA:V) of $0.1\,nm^{-1}$. When the egg yolk is heated, the phospholipid membrane becomes more permeable and releases its fat content, pictured in Fig. 7(b). The free-floating fat merges into larger fat bubbles with a much smaller SA:V. Because phospholipids are amphiphilic, they aggregate at the water-oil-interface. This creates a pressure on the shape of the globules to increase the SA:V, see Fig. 7(c). Note the scale bar indicating that these globules are much larger than the original lipoproteins. Ultimately, to maximize the surface area, the globules become shells, illustrated in Fig. 7(d). Without other influences, the SA:V of the shell at the end of the globule evolution would be the same as in the original lipoproteins.

5. Conclusion

Using x-ray holo-tomography, we successfully imaged the structure of protein networks and lipid globules in heat-treated egg yolk. Due to the large penetration depth of x-rays, these measurements did not require extensive sample preparation or fixation. We achieved a resolution of around 200 nm and could measure heating-time dependent

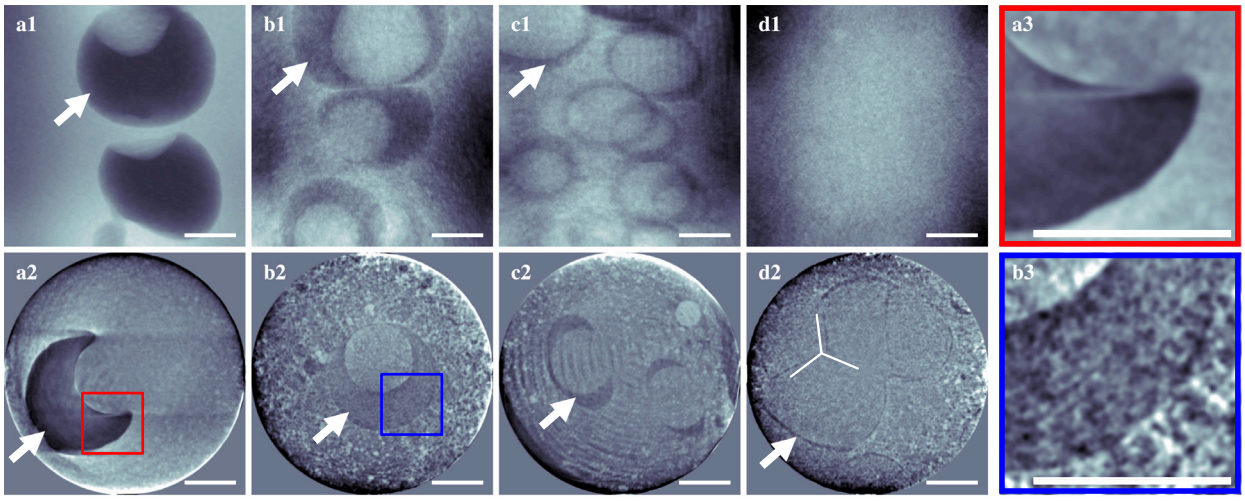

Fig. 6. Egg yolk samples with lipid globules arranged according to the estimated evolution. Arrows indicate exemplary globules. (a1–d1) show projections of the samples. (a2–d2) show horizontal slices through the sample. The horizontal stripes in (a2) are reconstruction artifacts caused by small sample changes during the measurement. (d2) contains a marker indicating the 120° intersection angles. (a3–b3) show enlarged sections for the first two samples to highlight how the protein network extends through the globules. All scale bars indicate 20 µm. The color scale of each image is individually optimized for best contrast.

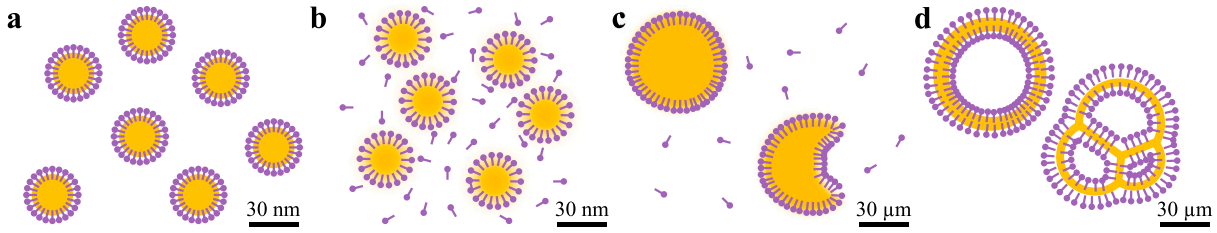

Fig. 7. Hypothesized evolution of the lipid globules in heat-treated egg yolk. (a) Lipoproteins in raw egg yolk. (b) At high temperatures, the phospholipid membrane becomes permeable and the fat leaks out. (c) Large fat droplets have a smaller surface-to-volume ratio, inducing shape changes. Note: length scale has changed. (d) Ultimately, the globules become hollow shells filled with egg yolk gel.

network structures in egg yolk, revealing a strong heterogeneity between samples. This sample-to-sample variation made it challenging to establish precise trends for different heating-times.

The heat-treatment of the egg yolk also caused the fat in the lipoproteins to transform into lipid globules up to tens of micrometers in diameter. Between samples, the shape of the globules varied, from spherical to hollowed-out and shell-like. Within each sample, the globules showed very similar shapes, hinting at a common evolution from a convex to a bubble-like form. This behavior is probably caused by the dissolution of lipoproteins at high temperatures, leading to an out-flow of fat that accumulates into globules which then transform into the bubbles. Fully understanding this effect requires further investigations. This transformation also showed a strong sample heterogeneity, as some samples showed no lipid agglomeration. To address the challenges caused by sample-to-sample variations, it will be necessary to use in-situ measurements to study the egg yolk during heating and follow the complete transformation of each sample.

CRediT authorship contribution statement

Felix Wittwer: Writing – review & editing, Writing – original draft, Software, Investigation, Formal analysis. **Nimmi Das Anthuparambil:** Writing – review & editing, Writing – original draft, Methodology, Investigation, Conceptualization. **Frederik Unger:** Writing – review & editing, Investigation. **Randeer Pratap Gautam:** Writing – review & editing, Investigation. **Silja Flenner:** Writing – review & editing, Software, Resources. **Imke Greving:** Writing – review & editing, Resources. **Christian Gutt:** Writing – review & editing, Methodology, Conceptualization. **Peter Modregger:** Writing – review & editing, Methodology, Investigation, Conceptualization.

Declaration of competing interest

The authors declare that they have no known competing financial interests or personal relationships that could have appeared to influence the work reported in this paper.

Acknowledgments

We acknowledge the Helmholtz-Zentrum Hereon and DESY, members of the Helmholtz Association HGF, for the provision of experimental facilities. Parts of this research were carried out at the Imaging Beamline P05 at PETRA III. Beamtime was allocated for proposal I-20240551. This research was supported in part through the Maxwell computational resources operated at Deutsches Elektronen-Synchrotron DESY, Hamburg, Germany. C.G., N.A., R.G. and F.U. acknowledge funding via DAPHNE4NFDI (project 4602487), BMFTR (projects 05K24PSA, 05K22PS1, 05D23PS1, 05K25PS3, 05K25PS1) and DESY Center for Molecular Water Science (CMWS).

Appendix A. Supplementary data

Supplementary material related to this article can be found online at https://doi.org/10.1016/j.jfoodeng.2025.112916.

Data availability

Data will be made available on request.

References

Aguilar, J., Cordobés, F., Bengoechea, C., Guerrero, A., 2019. Heat-induced gelation of egg yolk as a function of pH. Does the type of acid make any difference? Food Hydrocolloids 87, 142–148. http://dx.doi.org/10.1016/j.foodhyd.2018.07.045.

Anthuparambil, N.D., Girelli, A., Timmermann, S., Kowalski, M., Akhundzadeh, M.S., Retzbach, S., Senft, M.D., Dargasz, M., Gutmüller, D., Hiremath, A., et al., 2023. Exploring non-equilibrium processes and spatio-temporal scaling laws in heated egg yolk using coherent X-rays. Nat. Commun. 14 (1), 5580. http://dx.doi.org/10.1038/s41467-023-41202-z.

Anthuparambil, N.D., Timmermann, S., Dargasz, M., Retzbach, S., Senft, M.D., Begam, N., Ragulskaya, A., Paulus, M., Zhang, F., Westermeier, F., et al., 2024. Salt induced slowdown of kinetics and dynamics during thermal gelation of egg-yolk. J. Chem. Phys. 161 (5), http://dx.doi.org/10.1063/5.0219004.

Anton, M., 2013. Egg yolk: structures, functionalities and processes. J. Sci. Food Agric. 93 (12), 2871–2880. http://dx.doi.org/10.1002/jsfa.6247.

Ball, P., 2011. Shapes, paperback ed. Nature's Patterns, Oxford Univ. Press, Oxford, Number 1.

Běhalová, H., Tremlová, B., Kalčáková, L., Pospiech, M., Dordevic, D., 2020. Assessment of the effect of secondary fixation on the structure of meat products prepared for scanning electron microscopy. Foods 9 (4), 487. http://dx.doi.org/10.3390/foods9040487.

Bellairs, R., 1961. The structure of the yolk of the hen's egg as studied by electron microscopy. J. Cell. Biol. 11 (1), 207–225. http://dx.doi.org/10.1083/jcb.11.1.207.

Cordobés, F., Partal, P., Guerrero, A., 2004. Rheology and microstructure of heat-induced egg yolk gels. Rheol. Acta 43 (2), 184–195. http://dx.doi.org/10.1007/s00397-003-0338-3.

Diaz, A., Trtik, P., Guizar-Sicairos, M., Menzel, A., Thibault, P., Bunk, O., 2012. Quantitative X-ray phase nanotomography. Phys. Rev. B 85 (2), 020104. http://dx.doi.org/10.1103/PhysRevB.85.020104.

Dora, J., Flenner, S., Lopes Marinho, A., Hagemann, J., 2024a. A Python Framework for the Online Reconstruction of X-Ray Near-Field Holography Data. Zenodo, http://dx.doi.org/10.5281/ZENODO.8349364.

Dora, J., Möddel, M., Flenner, S., Reimers, J., Zeller-Plumhoff, B., Schroer, C.G., Knopp, T., Hagemann, J., 2025. Model-based autofocus for near-field phase retrieval. Opt. Express 33 (4), 6641. http://dx.doi.org/10.1364/OE.544573.

Dora, J., Möddel, M., Flenner, S., Schroer, C.G., Knopp, T., Hagemann, J., 2024b. Artifact-suppressing reconstruction of strongly interacting objects in X-ray near-field holography without a spatial support constraint. Opt. Express 32 (7), 10801. http://dx.doi.org/10.1364/OE.514641.

Evans, R.J., Bauer, D.H., Flegal, C.J., 1974. The egg yolk very low density lipoproteins of fresh and stored shell eggs. Poult. Sci. 53 (2), 645–652. http://dx.doi.org/10.3382/ps.0530645.

Flenner, S., Hagemann, J., Storm, M., Kubec, A., Qi, P., David, C., Longo, E., Niese, S., Gawlitza, P., Zeller-Plumhoff, B., Reimers, J., Müller, M., Greving, I., 2022. Hard X-ray nanotomography at the P05 imaging beamline at PETRA III. In: Müller, B., Wang, G. (Eds.), Developments in X-Ray Tomography XIV. SPIE, San Diego, United States, p. 19. http://dx.doi.org/10.1117/12.2632706.

Flenner, S., Kubec, A., David, C., Storm, M., Schaber, C.F., Vollrath, F., Müller, M., Greving, I., Hagemann, J., 2020. Hard X-ray nano-holotomography with a fresnel zone plate. Opt. Express 28 (25), 37514. http://dx.doi.org/10.1364/OE.406074.

Gürsoy, D., De Carlo, F., Xiao, X., Jacobsen, C., 2014. TomoPy: a framework for the analysis of synchrotron tomographic data. J. Synchrotron Radiat. 21 (5), 1188–1193. http://dx.doi.org/10.1107/S1600577514013939.

Howells, M., Beetz, T., Chapman, H., Cui, C., Holton, J., Jacobsen, C., Kirz, J., Lima, E., Marchesini, S., Miao, H., Sayre, D., Shapiro, D., Spence, J., Starodub, D., 2009. An assessment of the resolution limitation due to radiation-damage in X-ray diffraction microscopy. J. Electron Spectrosc. Relat. Phenom. 170 (1–3), 4–12. http://dx.doi.org/10.1016/j.elspec.2008.10.008.

Hsu, K.-C., Chung, W.-H., Lai, K.-M., 2009. Histological structures of native and cooked yolks from duck egg observed by SEM and cryo-SEM. J. Agricult. Food Chem. 57 (10), 4218–4223. http://dx.doi.org/10.1021/jf900495n.

Huopalahti, R., Anton, M., López-Fandiño, R., Schade, R., 2007. Bioactive Egg Compounds. Vol. 5, Springer, Berlin.

Mine, Y., 2008. Egg Bioscience and Biotechnology. John Wiley & Sons.

Nikara, S., Ahmadi, E., Nia, A.A., 2020. Effects of different preparation techniques on the microstructural features of biological materials for scanning electron microscopy. J. Agric. Food Res. 2, 100036. http://dx.doi.org/10.1016/j.jafr.2020.100036.

Paganin, D.M., Pelliccia, D., 2021. X-ray phase-contrast imaging: a broad overview of some fundamentals. In: Advances in Imaging and Electron Physics. Vol. 218, Elsevier, pp. 63–158. http://dx.doi.org/10.1016/bs.aiep.2021.04.002.

van der Walt, S., Schönberger, J.L., Nunez-Iglesias, J., Boulogne, F., Warner, J.D., Yager, N., Gouillart, E., Yu, T., 2014. Scikit-image: image processing in Python. PeerJ 2, e453. http://dx.doi.org/10.7717/peerj.453.

Withers, P.J., Bouman, C., Carmignato, S., Cnudde, V., Grimaldi, D., Hagen, C.K., Maire, E., Manley, M., Du Plessis, A., Stock, S.R., 2021. X-ray computed tomography. Nat. Rev. Methods Primers 1 (1), 18. http://dx.doi.org/10.1038/s43586-021-00015-4.